Physically Crosslinked Nanocomposites from Silicate-Crosslinked PEO: Mechanical Properties and Osteogenic Differentiation of Human Mesenchymal Stem Cells

Akhilesh K. Gaharwar,* Vipuil Kishore, Christian Rivera, Whitney Bullock, Chia-Jung Wu, Ozan Akkus, Gudrun Schmidt

The mechanical and biological properties of silicate-crosslinked PEO nanocomposites are studied. A strong correlation is observed between silicate concentration and mechanical properties. In vitro cell culture studies reveal that an increase in silicate concentration enhances the attachment and proliferation of human mesenchymal stem cells significantly. An upregulation in the expression of osteocalcin on nanocomposites compared to the tissue culture polystyrene control is observed. Together, these results suggest that silicate-based nanocomposites are bioactive and have the potential to be used in a range of biotechnological and biomedical applications such as injectable matrices, biomedical coatings, drug delivery, and regenerative medicine.

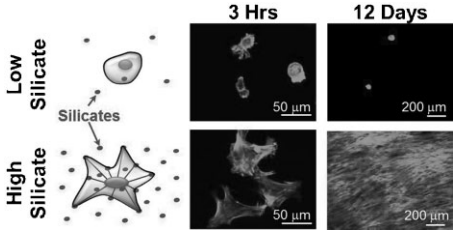

1. Introduction

Bioactive nanomaterials and polymer nanocomposites are currently the development focus of advanced biomaterials designed for emerging biotechnological applications such as nanomedicine, biomedical imaging, controlled drug delivery, and regenerative medicine.[1–6] A nanocomposite approach can be used to fabricate high-performance biomaterials with tailored physical, chemical, and biological properties.[5–9] Unique property combinations can be achieved by controlling the interactions between polymer and nanoparticles.[10–15] The fundamental understanding and knowledge of the nanoscale structures are necessary to tailor the macroscale material properties for the desired biomedical applications.

Dr. A. K. Gaharwar, Dr. V. Kishore, C. Rivera, W. Bullock, C.-J. Wu, Prof. O. Akkus, Prof. G. Schmidt
Weldon School of Biomedical Engineering, Purdue University, West Lafayette, IN 47907-2032, USA
E-mail: agaharwa@purdue.edu

A. K. G. and V. K. contributed equally to this work.

Silicate-based polymer nanocomposites have shown promise as the next generation bioactive materials for drug delivery, biomedical imaging and tissue engineering applications due to the enhanced surface interactions of polymer chains and silicate nanoparticles.[4,7,16–19] Synthetic silicates such as Laponite ($Na^{+}_{0.7}[(Mg_{5.5}Li_{0.3})Si_8O_{20}(OH)_4]^{-}_{0.7}$) are similar in chemical composition to bioactive glasses (SiO_2, Na_2O, CaO, MgO, P_2O_5) and thus can mimic some of their biological properties.[20–22] Furthermore, Laponite has been shown to degrade/dissolve into non-toxic products [Na^{+}, $Si(OH)_4$, Mg^{2+}, Li^{+}] at pH values between 7.3 and 8.4.[23] Orthosilicic acid [$Si(OH)_4$], one of the major dissolution products of silicate, has been shown to be absorbed by the human body.[24,25] Orthosilicic acid is also found in numerous human tissues and organs such as bone, tendon, aorta, liver tissues, and kidney tissues.[24,25] Further, orthosilicic acid promotes collagen type I synthesis and osteoblastic differentiation in human osteosarcoma cells (MG-63) in vitro.[26]

In a recent study, Li et al. proposed the use of alginate gels, containing Laponite nanoparticles, for the controlled delivery of cationic drugs.[27] They showed that cationic

DOI: 10.1002/mabi.201100508

macromolecules strongly interacted with the nanoparticles surface and exhibited pH-dependent release profiles.[27] In another approach, Tzitzios et al. immobilized magnetic nanoparticles on Laponite for magnetic resonance imaging (MRI) applications.[28] The hybrid ferrofluid (containing Laponite and magnetic nanoparticles) showed a significantly higher saturation magnetization than the ferrofluid (containing only magnetic nanoparticles) mainly due to the higher loading efficiency of magnetic nanoparticles on Laponite surfaces and to the suppression of the magnetic interparticle interactions.

Pek et al. proposed to use the thixotropic characteristic of nanocomposite hydrogels for three dimensional cell culture[29] and showed that the addition of a high amount of silica nanoparticles not only mechanically reinforced the polymeric hydrogel but also facilitated the differentiation of human mesenchymal stem cells (hMSCs) into osteogenic lineage.[29] The addition of silicate has also been shown to significantly enhance the adhesion of hMSCs on mechanically robust PEG hydrogel surfaces.[30]

Population of constructs with cells prior to implantation is a viable strategy to promote bone formation in vivo. There are three main cell sources that can be used for bone tissue engineering applications: (i) differentiated osteoblasts, (ii) embryonic stem cells (ESCs), and (iii) mesenchymal stem cells (MSCs). Although using differentiated osteoblasts obtained from autologous bone biopsies is the primary choice, the applicability of differentiated osteoblasts in bone tissue engineering has several limitations: (i) dedifferentiation of osteoblasts leading to loss in specialized function, (ii) short survival time in culture, and (iii) relatively low cell yield from biopsies. Alternative sources like ESCs have enormous potential; however, differentiating them to specific lineages is a challenge due to extensive pluripotency. Additionally, they are associated with ethical concerns and risk of teratoma formation. MSCs have gained considerable interest for bone tissue engineering applications because of the following advantages: (i) availability of multiple sources for isolation for example: bone marrow, adipose, umbilical cord blood, (ii) ease of isolation and, (iii) protocols for osteogenic differentiation of MSCs are well established, and (iv) identification of specific markers (CD90, CD105, CD73) for MSCs have made them a reliable source. While we have previously reported that silicate nanoparticles (Laponite RD) effectively control the adhesion, proliferation, and differentiation of preosteoblast cells on silicate crosslinked PEO nanocomposites, the in vitro response of MSCs to this novel nanocomposite is unknown. Therefore, in this study, the potential of silicate crosslinked PEO nanocomposites to induce osteogenic differentiation of hMSCs was investigated.

We have previously reported that silicate nanoparticles (Laponite RD) enhance the mechanical properties of poly(ethylene oxide) (PEO) nanocomposites and can be used to effectively control the adhesion, spreading, and proliferationof fibroblast and preosteoblast cells on silicate crosslinked PEO surfaces.[31,32] In this study, the concentration of silicate nanoparticles within the PEO was varied and its effect on the mechanical and structural properties of nanocomposite hydrogels and dry films made from hydrogels was investigated. Furthermore, hMSCs were seeded onto silicate crosslinked PEO films and the effect of silicate on adhesion, spreading, proliferation, and osteogenic differentiation potential of hMSCs was investigated.

2. Experimental Section

2.1. Preparation of Nanocomposites

PEO with $\overline{M}_w = 10^6\,g \cdot mol^{-1}$ and a molecular mass distribution of 1.5 was purchased from Polysciences Inc. Laponite (LRD) from Southern Clay Products Inc. is a synthetic Hectorite type silicate consisting of nanoplatelets with an average diameter of 25–30 nm and a thickness of ≈1 nm. Preparation of nanocomposite hydrogels and films is shown in Figure 1. Nanocomposite hydrogels were prepared via a gel/solution exfoliation method by dissolving 5–*X* wt% PEO and *X* wt% LRD in 95% water.[33,34] Vigorous mixing was required to obtain fully exfoliated hydrogels. Nanocomposite films were prepared by spreading the hydrogels onto glass slides and drying at 25 °C in desiccators and subsequently under vacuum.[35,36] The composition of films after solvent evaporation was calculated from the initial weight of polymer and silicates (by mass fraction). After drying, 10 manually spread layers gave 70–100 μm thick films depending upon the concentration of the gels.

2.2. Rheological Properties of Nanocomposite Hydrogels

Rheological properties of nanocomposite hydrogels were determined using an AR2000 stress controlled rheometer and ARES strain controlled rheometer (TA Instruments Ltd.) ($n = 3$). Flow experiments were performed by measuring the viscosity (in Pa s) as a function of shear rate (0.01–100 s^{-1}). Hysteresis experiments were performed by subjecting the nanocomposite sample to increasing shear rates, from 10 to 500 s^{-1}, for 10 s per shear rate over a period of 10 min to generate the "up" curve. The samples were held at the maximum shear rate for 10 s before the shear rate was decreased back to 10 s^{-1} over a period of 10 min to generate the "down" curve. Stress sweep and frequency sweep were performed at 37 °C. Storage modulus (G'), loss modulus (G''), and tan delta (δ) were determined using stress sweep (0.01–1000 Pa, 1 Hz), frequency sweep (0.01–100 Hz, 10 Pa), and strain sweep (0.01–10%, 1 Hz). Flow experiments determined the effect of viscosity on shear rate. All tests were performed using a 40 mm parallel plate geometry and a gap of 500 μm. A solvent trap was used to minimize solvent evaporation.

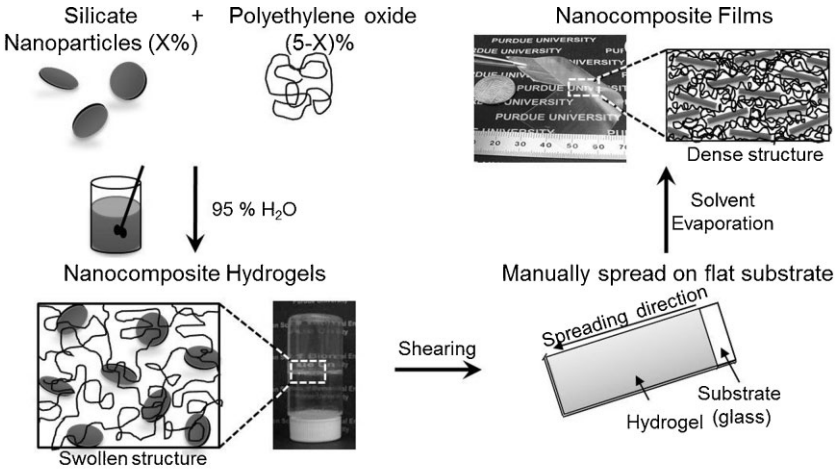

Composition of Nanocomposite Hydrogels

Sample	Silicate (%)	PEO (%)	Water (%)
2.0 % Silicate	2	3	95
2.5 % Silicate	2.5	2.5	95
3.0 % Silicate	3	2	95
3.5 % Silicate	3.5	1.5	95

Composition of Nanocomposite Films

Sample	Silicate (%)	PEO (%)
40 % Silicate	40	60
50 % Silicate	50	50
60% Silicate	60	40
70% Silicate	70	30

Figure 1. Preparation of physically crosslinked PEO/silicate nanocomposite hydrogels and films. Hydrogels were prepared by mixing the required amounts of silicate nanoparticles and PEO in 95% water. Vigorous mixing was required to obtain fully exfoliated hydrogels. The swollen hydrogel network was subjected to shearing and solvent evaporation, in order to obtain dense nanocomposite films. The compositions of nanocomposite hydrogels and dried films are listed in weight percentage.

2.3. Structural Characteristics of Nanocomposite Films

Raman spectroscopy was used to follow the formation of PEO crystallites in the nanocomposite films.[37,38] The Raman system (LabRam, Jobin-Yvon Horiba Inc., Edison, NJ, USA) consisted of a microscope (Olympus BX41), a stigmatic Raman spectrometer, a computer controlled *xy* stage for sample positioning and a laser source (633 nm Helium-Neon laser). Two scans with a detector signal accumulation time of 60 s · $scan^{-1}$ provided a good signal-to-noise ratio of Raman bands. Other parameters were: confocal hole size of 1100 μm, a slit width of 250 μm, a 600 g · mm^{-1} grating and a 10× objective. Spectral data were baseline corrected with a 5° polynomial. Microstructures of nanocomposite films were observed using a JEOL JSM-840 scanning electron microscope. The cross-section of nanocomposites films was freeze fractured using liquid nitrogen and later sputter coated with platinum at −130 °C for 90 s.

2.4. Mechanical Properties of Nanocomposite Films

Mechanical testing was done using an LE3-2 system from Test Resources Inc. LVDT output was used to control the actuator. Stress/strain curves were obtained by testing ≈3 mm wide, ≈70–100 μm thick, and ≈15 mm long samples from films cut in the spreading direction. The strain rate was set at 10 mm · min^{-1} for all experiments. The grip regions were reinforced with paper to reduce the possibility of failure. The ultimate tensile strength (UTS) was expressed in MPa and calculated by dividing the maximum load (N) by the initial cross-sectional area (m^2) of the specimens. The elongation at break was calculated as the ratio of the final length at the failure to the initial length (10 mm) and expressed as a percentage. Elastic modulus was calculated from the slope of the linear elastic region of stress/strain curves. Tests were repeated five times for each nanocomposite composition.

2.5. Adhesion, Spreading, and Proliferation of hMSCs on Silicate-Crosslinked PEO Films

The nanocomposite films with different concentration of silicate (40, 50, 60, and 70%) were cut into 1.5 cm disks, sterilized by briefly submerging in 70% ethanol, washed with 1× PBS and placed individually into each well of an ultralow attachment 24 well plate (Corning). To evaluate the effect of silicate concentration on cell adhesion and proliferation, passage-5 hMSCs (Lonza) were seeded onto silicate crosslinked PEO nanocomposites at a density of 5000 cells · cm^{-2} and cultured for 12 d. Tissue culture polystyrene surface (TCPS) was used as a positive control. The culture medium composed of minimal essential medium (MEM) alpha medium with 10% fetal bovine serum and 1% penicillin/streptomycin. At periodic intervals, cell proliferation was quantified using alamar blue assay by following manufacturer's instructions. Briefly, 0.5 mL of alamar blue mix (culture medium + 10% alamar blue) was added to each well and incubated for 2 h at 37 °C. Following this, 100 μL of alamar blue mix from each well was transferred to a 96 well plate in triplicate and the absorbance was recorded at 570 and 600 nm. Cell number was quantified by calculating the percentage reduction in alamar blue and comparing the values to a standard curve generated using known number of cells. Cell adhesion was determined as the ratio of the number of cells calculated using alamar blue assay four hours after seeding to the initial seeding density. Cell morphology and spreading was evaluated by seeding hMSCs at a density of 7 500 cells · cm^{-2} on the nanocomposites films. Four hours after seeding, cells were fixed in 3% formaldehyde (with 0.1% TritonX-100) and the actin filaments were stained with AlexaFluor Phalloidin to visually examine cell attachment and morphology. High quality images were taken using confocal microscopy (Olympus FV1000).

2.6. Osteogenic Differentiation of hMSCs on Silicate-Crosslinked PEO Nanocomposites

To examine the osteogenic differentiation potential of silicate crosslinked PEO nanocomposite films, hMSCs (P5) were seeded at a

density of 5000 cells $\cdot$ cm^{-2} and cultured for 10 d. The culture medium composed of alpha-MEM with 10% FBS, 1% penicillin/streptomycin, 0.01 M β-glycerophosphate, and 0.284×10^{-6} M ascorbic acid. At periodic intervals (day 7 and day 10), total RNA was extracted by lysing the cells using TRIZOL reagent (Invitrogen) and following the manufacturer's protocol. Following this, cDNA was synthesized from the total RNA using the high-capacity cDNA reverse transcription kit (Applied Biosystems). Taqman gene expression assays (Applied Biosystems) for runx2, osteocalcin and β-actin (endogenous control) were used to evaluate the expression of the genes by quantitative reverse transciprtion polymerase chain reaction (RT-PCR) (Applied Biosystems 7500 Real Time PCR System). The relative fold change in target gene expression was quantified using the 2deltadeltaCt method by normalizing the target gene expression to β-actin and relative to the expression at day 7 on the TCPS control.

2.7. Statistical Analysis

Data are presented as mean $\pm$ standard deviation of the mean values. Statistical analysis was performed using Minitab (version 16, Minitab Inc, USA) to determine the statistical differences. Statistical comparisons were performed with one-way analysis of variance (ANOVA) for an average of 3–5 replicates. After ANOVA was performed on the dataset, Tukey's method was used to test all pair wise mean comparisons. Statistical significance for all tests was set at a p-value < 0.05.

3. Results and Discussion

Synergistic combinations of flexible polymers and hard nanoparticles are capable of mimicking material properties and biological aspects of natural materials. By controlling physical interactions between silicate nanoparticles and PEO chains, viscoelastic, injectable, and tough matrices can be fabricated. These physically crosslinked hydrogels do not require any additional photo/chemical initiator or exposure to harmful ultraviolet radiations and have potential for encapsulating cells for 3D cell culture and tissue engineering. Highly extensible and dense nanocomposite films can also be obtained by subjecting the fully exfoliated hydrogels to solvent evaporation. The mechanical properties of nanocomposites strongly depend on silicate concentration. As expected a strong correlation between silicate concentration, microstructural, and mechanical properties was observed in the nanocomposites.

3.1. Physically Crosslinked Nanocomposite Hydrogels

Structural information at the micrometer length scale is important when designing nanocomposites and is critical when formulating them into mechanically strong functional materials. Nanocomposite hydrogels were prepared by mixing the appropriate amount of PEO and silicate nanoparticles in 95% water (Figure 1). A fully exfoliated nanocomposite network was obtained by vigorous mixing. To determine the injectibility of nanocomposite hydrogels, viscosity measurements were performed. Figure 2a indicates that all the nanocomposite hydrogels shear thin into low viscous liquids under deformation. At low shear rates, the silicate concentration significantly affected the viscosity of the hydrogels, whereas at the higher shear rates no significant change in viscosity was observed with composition. Power law exponents [$\eta = (d\gamma/dt)\ m$] of hydrogels were in the following range: $m = -0.64$ for 2% silicate, $m = -0.70$ for 2.5% silicate, $m = -0.73$ for 3% silicate, and $m = -0.77$ for 3.5% silicate. The power law exponents obtained in this study are comparable to the results reported by Schmidt et al. and Baghdadi et al. on other PEO/Laponite hydrogel systems.[33,39–41]

The injectable hydrogels have potential to be used as matrix for delivery of therapeutic agents.[42–44] The silicate-based hydrogels can shear-thin when subjected to the appropriate shear (Figure 2a). After removal of shear forces, the hydrogels immediately recover their stiffness. Moreover, the silicate-based hydrogels are formed due to physical interactions and not by covalent crosslinking thus eliminating any in vitro-biocompatibility issues related to unreacted monomer or initiator. However, only in vivo studies can determine if these materials are biocompatible by definition, thus do no harm to the patient. We also observed that the silicate-based hydrogels retained their shape when subjected to physiological conditions [phosphate-buffered saline (PBS). Samples are stable at room temperature and do not need specific storage facilities. When these hydrogels are subjected to distilled water, the network quickly dissolves or disintegrates. Preliminary results suggest that the dissolution behavior of these nanocomposite hydrogels can be controlled by changing the ionic strength of the solvent (data not shown). The potential application of these hydrogels includes the controlled delivery of entrapped macromolecules as they exhibit stimuli-responsive swelling behavior.

3.2. Effect of Silicate on Recovery of Hydrogel Network

Hydrogels with shear thinning and self-healing properties are suitable candidates for injectable therapeutic delivery vehicles.[42–44] By monitoring the recovery of the hydrogel network after flow or shear deformation one can provide information on how fast the network recovers, and one can evaluate the ability of the hydrogel to remain localized after injection.[45] The effect of silicate on recovery of the hydrogel network was estimated from the hysteresis experiments (Figure 2b). In these experiments, the effect of cyclic increase and decrease of shear rate on the viscosity of the hydrogel network was evaluated. The area between the curves (loading and unloading cycles) was used to

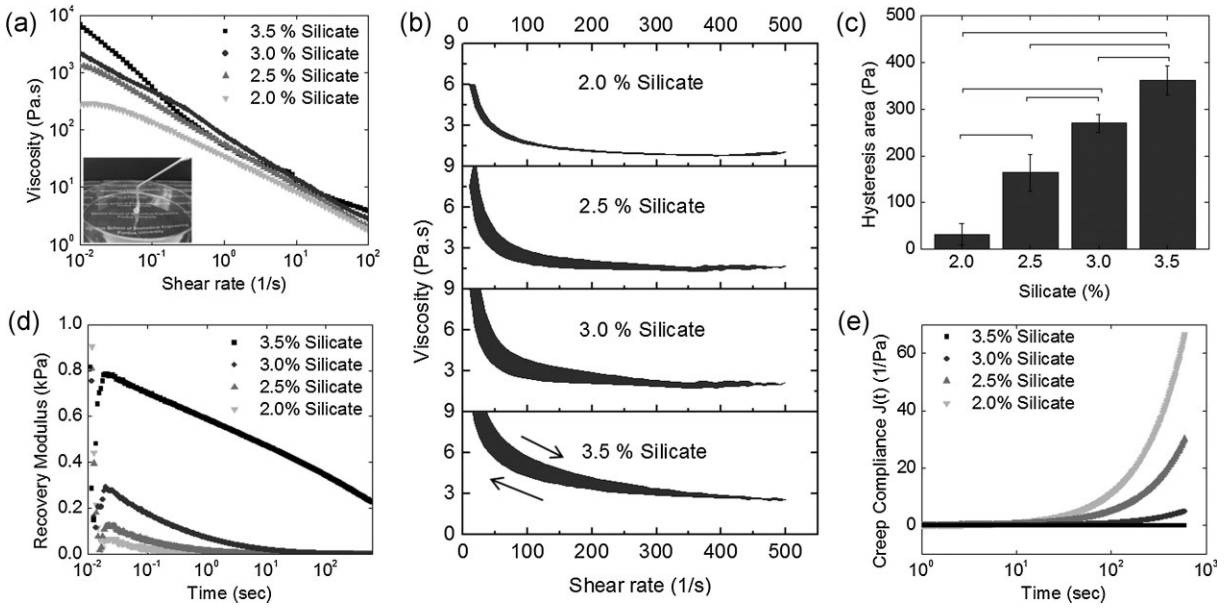

Figure 2. Effect of silicate on hydrogel network structure and its recovery. (a) The injectibility of nanocomposite hydrogels was determined by flow experiments. All the hydrogels show shear thinning behavior. The viscosity of the hydrogels decreased with increase in shear rate. (b,c) Effect of silicate on recovery of hydrogel network was obtained by hysteresis experiments. The hydrogel networks were subjected first to an increasing shear rate and then to a decreasing shear rate. The area between the loading and unloading curve indicates the extent of network recovery. We find that an increase in silicate concentration decreases network recovery, indicating that polymer physically interacts with silicate surfaces. (d,e) In mechanical testing, relaxation moduli, and creep compliances [$J(t)$] decrease with increase in silicate concentration. This further indicates the formation of physically crosslinked network between silicate and polymer chains. Statistical significance ($p < 0.05$) between the groups is indicated by bars.

determine the hysteresis of the sample which is a measure of the network's ability to recover. For example, the smaller hysteresis indicates a faster recovery of the hydrogel network. This is most likely due to the presence of a lower number of physical crosslinking sites. Figure 2b and c show that at lower silicate concentrations, the network recovered faster due to the presence of excess polymer and lower degree of crosslinking, whereas slower network recovery was observed at higher silicate concentrations.

Time/dependent recovery of the nanocomposite network was evaluated from stress-relaxation experiments. In these experiments, the recovery of the nanocomposite network under constant strain was investigated. Figure 2d shows that instantaneous stress exerted by the nanocomposite network is proportional to the amount of silicate. The network relaxes with time and the rearrangement of polymer chains and nanoparticles helps in the dissipation of stress within the network. In creep experiments, the hydrogel network was subjected to a constant shear stress and the shear strain of the material was monitored as a function of time. Creep compliance [$J(t)$] data as a function of time are presented in Figure 2e. Nanocomposites, containing low silicate concentration, yield quickly under the applied stress. With an increase in silicate concentration, the network becomes more rigid and resists the applied shear stress. This indicates that silicate acts as a physical (non-covalent) crosslinker which reinforces the polymer network.

Overall, these experiments suggest that the addition of silicate nanoparticles to PEO increases the crosslinking density and enhances the network stability of nanocomposite hydrogels. Comparable results were reported by Schmidt et al. and Baghdadi et al. on different hydrogel compositions.[33,39–41] They reported that polymer chains attach and detach to the silicate in dynamic equilibrium forming a viscoelastic network.[34,46,47] According to these studies the edges of the silicate nanoplatelets have a higher polymer density compared to the faces. Thus, multiple polymer chains may attach to the same or different nanoparticle crosslinkers while forming a network.[47] Under shear deformation, the viscoelastic network breaks and the hydrogel starts to flow. After cessation of stress, the network structure recovers and the hydrogel regains its rigidity.[34,46,47]

Although the ability of the hydrogel network to recover from the applied deformation is strongly dependent on the polymer to silicate ratio, regardless of their composition all hydrogels recover to their original stiffness after cessation of the stress. This indicates that silicate-based hydrogels can be injected into a defect site to readily fill up the void space suggesting potential application for minimally invasive therapies.

3.3. Rheological Properties of Nanocomposite Hydrogels

Evaluation of rheological properties of hydrogels is important to determine the suitability of the materials for specific biotechnological use. For example, hydrogels with low viscosity can be used as injectable scaffolds for gap-filling or for delivery of bioactive molecules or cells; whereas, more viscous hydrogels can be considered for soft tissue repair.[48,49]

Rheological properties of the hydrogel networks can be determined using the viscoelasticity theory (time-dependent recovery of orientations and structure).[50] Here, we have used oscillatory sweep experiments to investigate structural integrity and mechanical properties of the physically crosslinked hydrogels (Figure 3). In these experiments, hydrogels were subjected to an oscillating shear strain, stress, or frequency (at 37 °C), and the material responses were measured. Results show that the addition of silicate significantly influences the viscoelastic properties of the hydrogel networks.

Stress sweep experiments were first performed to determine the linear viscoelastic region (LVR). Figure 3a shows that all the nanocomposites show an LVR between 0.01 and 10 Pa stress. The storage modulus (G') for samples, containing 2.5, 3, and 3.5% silicate, is greater than their loss modulus (G''). Moreover, with an increase in silicate concentration, the difference between storage modulus and loss modulus increases, indicating solid-like behavior.

Similar trends were observed in strain sweep experiments (Figure 3b). All of the hydrogels display an LVR at low strains (0.01–1.0%). At high strains (≈10%), a rapid decline in elastic modulus (G') was observed, indicating disruption of the network structure (Figure 3b). The addition of silicate nanoparticles to the polymeric hydrogel matrix increases the elastic modulus and decreases tan δ. Silicate also increases the cross-over strains and cross-over moduli. This indicates that the addition of silicate reinforces the polymer network and causes the hydrogel to display a solid-like behavior.

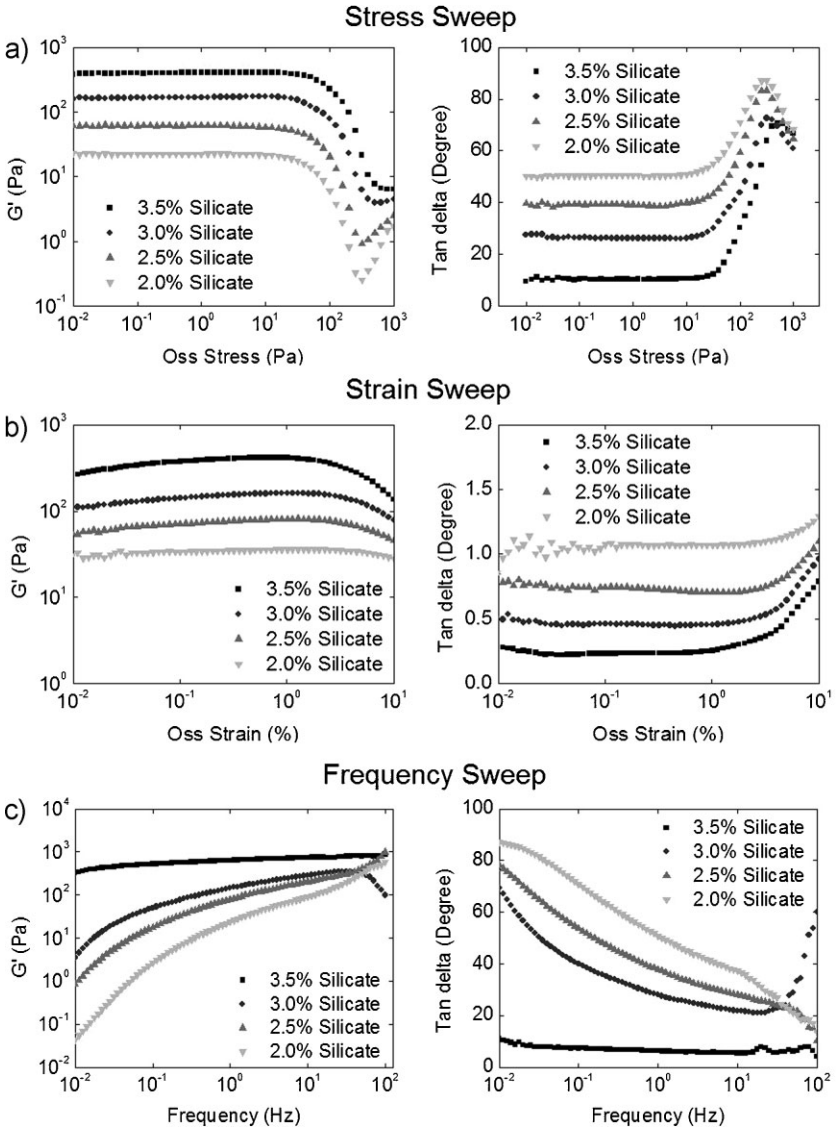

Figure 3. Effect of silicate nanoparticles on the rheological properties of hydrogels. (a) Stress sweep experiment show that the elastic moduli (G') of the nanocomposite hydrogels increase and tan delta decrease with increase in silicate concentration. The presence of an LVR indicates stability of network structure under stress. All the networks start to yield around a shear stress of 100 Pa. The presence of cross-over stress increases with increase in silicate concentration indicating formation of stable network. Similar results were obtained in (b) stain sweep and (c) frequency sweep experiments. This indicates that silicate nanoparticles act as physical crosslinkers and reinforces the network.

The dependence of storage (G') and loss (G'') moduli on frequency is shown for different concentrations of silicate/PEO (Figure 3c). Trends suggest that the storage modulus (G') increases and tan δ decreases with an increase in silicate concentration. This is mainly attributed to the increase in crosslinking density due to enhanced surface interactions between PEO and silicate nanoparticles. At a lower silicate concentrations, G' decreases with an increase in frequency;

whereas, at a higher silicate concentrations (3.5% silicate), G' becomes independent of the applied frequency. This indicates the transition from a liquid-like to a solid-like state. Similar results were reported by Zhang and Archer for other PEO/silica nanocomposites.[51] This group showed that the addition of silica nanoparticles strongly influences the stress relaxation dynamics. Loiseau and Tassin observed similar behavior in other PEO/silicate nanocomposite hydrogels.[52] These researchers observed an increase in elastic moduli with a power law of the frequency.

Overall, the observed behavior can be attributed to the formation of physically crosslinked networks and to the enhanced surface interactions between silicate nanoparticles and polymer chains (Figure 4). It has been reported that PEO physically adsorbs onto silicate nanoparticles and forms a core/shell structure.[41,53–55] The exact interactions between silicate and polymer chains are not known, but most of the researchers believe that hydrogen bonding, ionic, dipole, and other interactions might play a role in the formation of these physically crosslinked networks.[7] The physical interactions result in formation of a compact and dense layer of train and loops on the surfaces of the silicate nanoparticles.[54,55] If the polymer chains are long enough, they interconnect multiple nanoparticles, which results in the formation of physically crosslinked networks.[53] The addition of silicate nanoparticles effectively restricts the relaxation of polymer chains, that are crosslinked between the silicate nanoparticles, and effectively increases the elastic modulus. At rest, silicate nanoparticles are randomly oriented within the matrix and, polymer chains form coils and loops. During mechanical deformation, those polymer chains, that are crosslinked between the nanoparticles, will stretch. An increase in silicate concentration results in higher cross-link densities and highly viscous hydrogels. The mechanical properties of these hydrogels can be further tuned by changing pH and ionic strength.[56]

Comparable trends were observed by Tigges et al. for different PEG/silica nanocomposite hydrogels.[57] They reported that addition of silica nanoparticles to star-shaped PEO hydrogels enhanced both the hardness and the modulus by threefold, when compared to pure polymer hydrogel.[57] In another study, Lin et al. showed that physical interactions between polymer chains and surfaces of nanoparticles (silica), increased toughness, and moduli by several folds.[58] They also observed that a large increase in mechanical properties was not observed when polymer chains did not interact with the nanoparticles.

3.4. Physically Crosslinked Dried Nanocomposite Films

The structure and physical properties of dried nanocomposite films are important to assess their suitability for various biotechnological applications such as erodible biomedical coatings, drug delivery, biosensors, and tissue engineering constructs. In general, properties of biomedical materials are determined under physiological conditions (limited temperature, pH range, and ionic concentration). Although some of the mechanical properties of the dried films are diminished when immersed in phosphate buffer solution, it is also important to evaluate the materials properties in the dry state. For example, if these nanocomposites are to be used for developing wound healing patches, we can entrap protein or peptide within the hydrogel network, then dry it to obtain dense nanocomposite films. When the dried nanocomposite film comes in contact with biological fluid it will swell and release the entrapped macromolecule to obtain relevant therapeutic effect.

Dense nanocomposite films were obtained by subjecting the fully exfoliated hydrogel to shearing and solvent evaporation (Figure 1). Upon drying, the swollen hydrogel structure collapsed and translucent or transparent nanocomposite films were formed. Addition of silicate significantly influenced the opti-

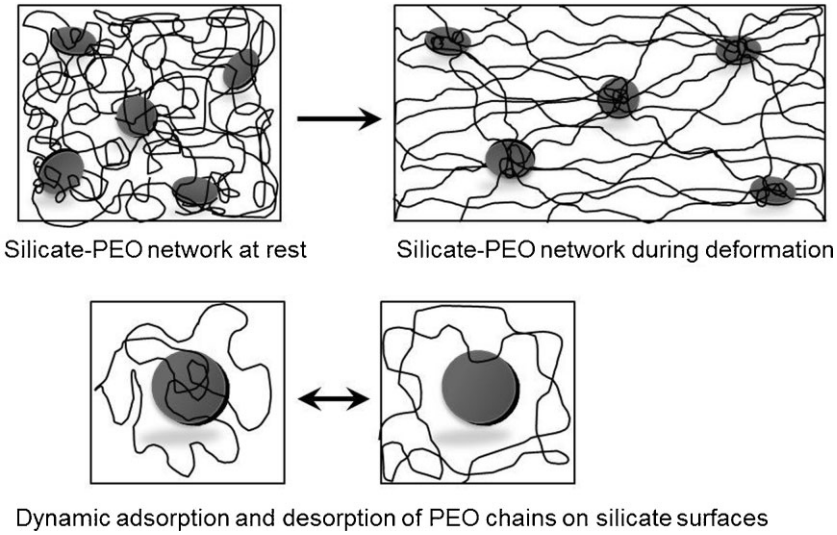

Figure 4. Schematic showing the effect of mechanical deformation on network structure of nanocomposite hydrogel. Silicate nanoparticles are physically crosslinked to PEO chains and form a viscoelastic network. The polymer chains physically adsorb and desorb on the silicate surfaces due to hydrogen bonding and ionic interactions. At rest silicate particles are randomly oriented within the matrix and polymer chains form coils and loops. When the physically crosslinked network is subjected to mechanical deformation, polymer chains undergo stretching. Under mechanical loading, silicate particles act as reversible physical crosslinkers that restrict polymer chain movements and reinforce the hydrogel network.

cal properties of the nanocomposite films (Figure 5a and b). To quantify these optical properties, transmittance spectra of films at different wavelengths were obtained. The nanocomposite films, containing 70% silicate, transmit almost 90% of the incident light. This is attributed to suppressed crystallization and formation of amorphous polymer in the presence of silicate. Thus, addition of silicate facilitates transmission of light.

3.5. Raman Spectroscopy of Dried Nancomposite Films

Raman spectra from nanocomposites containing different amounts of silicate were obtained to determine the crystalline and amorphous contributions of PEO in the dried state (Figure 5c and d). Koenig et al. reported Raman spectra from crystalline PEO, molten PEO, and PEO solutions and delineated contributions from crystalline and amorphous PEO.[56] This group found that the crystalline PEO displayed band splitting, whereas, single and diffused bands were observed for amorphous PEO. Our results from crystalline PEO correlate with the literature.[56,59] The observed bands are assigned to the different vibration modes in Figure 5d. Dried PEO films displayed band splitting at 278, 368, 537, 842, 1062, 1142, 1233, 1282, 1453, 1486 cm^{-1}. Addition of silicate significantly influenced the size and shape of the Raman bands. The band splitting disappeared with an increase in silicate concentration, indicating a loss of polymer crystallinity.

The decrease in polymer crystallinity in a dried state can be directly related to the interaction between silicate nanoparticles and polymer chains. Polymer, that is adsorbed on the surface or intercalated between silicate layers, is mostly amorphous. Whereas, free or excess polymer, that is not attached to silicate, is present in crystalline form. Nanocomposites containing 60 and 70% silicate do not show a single band splitting, indicating amorphous polymer structures. These results correlate with the polarized microscopy results reported earlier[60,61] and indicate that 40% PEO is sufficient to saturate the silicate surfaces.

3.6. Hierarchical Structures in Dried Nanocomposite Films

The structure of the nanocomposite films can significantly influences mechanical, chemical, and biological properties. Here, scanning electron microscopy was used to determine the structures of the nanocomposite films at a μm length scale. Figure 6 reveals a formation of a hierarchical structure

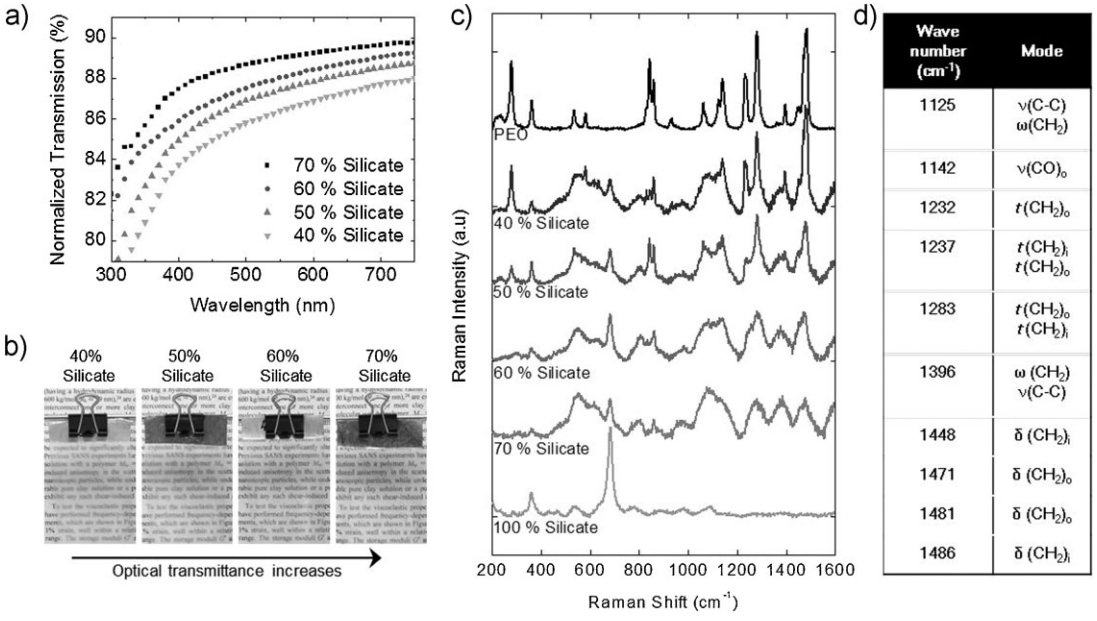

Figure 5. Effect of silicate on the optical properties of dried nanocomposite films. (a) Optical transmittance of nanocomposite films at different wavelengths. With increase in silicate concentration, optical transmittance increases. (b) Addition of silicate favorably alters the optical properties and films become more transparent at higher silicate concentration. The distance between the film and the background is ≈1 cm. (c) The Raman spectrum of silicate crosslinked nanocomposites. (d) The Raman bands are assigned to the different vibration modes of PEO. Mode assignments: ν (stretching), δ (bending), ω (wagging), τ (twisting). The Raman peak at 1396 cm^{-1} corresponds to the wagging of CH_2 and the stretching of C−C of PEO. The Raman spectroscopy can be used to monitor the PEO crystallinity in the nanocomposites. With increase in silicate concentration the Raman peaks at 1396 cm^{-1} decrease and completely disappears in the sample containing 60% silicate. This indicates that at and below 60% silicate concentration, the polymer is intercalated between silicate nanoplatelets and is present in amorphous form.

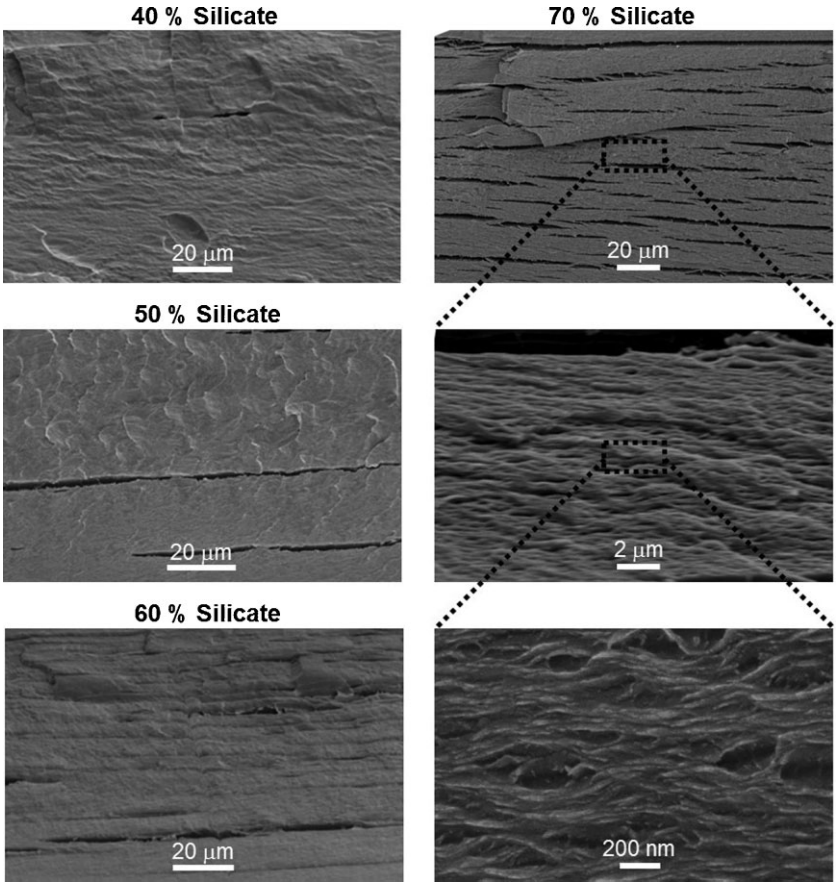

Figure 6. Effect of silicate on the microstructure of nanocomposite films. At low silicate concentrations (≈40%), dense and cohesive structures are observed due to substantial intermixing of polymer and silicate between the spread layers. At higher silicate concentrations (70%), hierarchical structures are observed on micrometer to nanometer length scales. The hierarchical structures observed in dried nanocomposite films containing 70% silicate can be compared to brick and mortar structure. Crack observed in the SEM images originates from freeze fracturing.

with an increase in silicate concentration. In nanocomposites containing 40% silicate, layered structure was not observed, indicating substantial intermixing and cohesiveness between two spread layers. On the other hand, microstructural evaluation of nanocomposites containing high silicate concentrations (70%), revealed the presence of several sub-layers within a single spread layer, indicating an ordered arrangement of Laponite and PEO at the nanoscale.

The microstructure of high silicate nanocomposite films is similar to that of nacre at μm length scale.[62,63] Both bone and nacre resist the initiation and growth of a crack by similar toughening mechanisms.[64] Here, the hierarchical structures of the nanocomposite films were obtained due to film fabrication process, which involves shearing and solvent evaporation. Similar results were reported earlier on nanocomposites containing 60% silicate and 40% PEO.[35,36] The hierarchical structures reported in nanocomposites containing 70% silicate (Figure 6) are denser and compact. Cracks observed in SEM images originate from freeze fracturing.

The ordered arrangement of polymer and silicate nanoparticles (especially in nanocomposite films containing high silicate concentrations) can be compared to brick and mortar structure. The hierarchical layered structure can also be used to store macromolecules or biomolecules for sustained delivery applications. Due to high ionic capacity of silicate nanoparticles, charged macromolecules can be immobilized on the nanoparticle surface. The dense and hierarchical structure can provide an additional shield to the entrapped macromolecules. Thus, one of the potential applications of these hybrid films can be in area of controlled drug delivery.

3.7. Silicate Improves the Mechanical Strength of Dried Nanocomposite Films

Mechanical properties of materials strongly influence biological properties. To determine the effect of silicate nanoparticles on the mechanical properties of dried nanocomposite films, uniaxial tensile tests were used to determine the ultimate strain and stress (Figure 7). All the nanocomposites showed a yield point and necking. The ultimate strength and ultimate elongation (Figure 7b and c) were calculated from the stress/strain plots. The ultimate stress for nanocomposite with low silicate concentration (40, 50, and 60%) was significantly different from nanocomposite films containing 70% silicate.

Nanocomposites containing low silicate concentration showed unusually high extensibility (≈700%). The total strains for all samples were significantly different from each other ($p < 0.05$), except the 40–50% silicate. Neither pure PEO, nor pure Laponite films, have such high extensibility. PEO is a flexible polymer, and silicate is responsible for crosslinking polymer chains to form a network, which is related to the high elongation. From polarized microscopy, highly aligned structure was observed in the stretched region at low silicate concentration (Figure 7d). Due to the high molecular weight of PEO, the polymer chains attach to multiple silicate particles and act as a flexible link.[53] During mechanical deformation, coiled polymer chains, that are crosslinked with the silicate

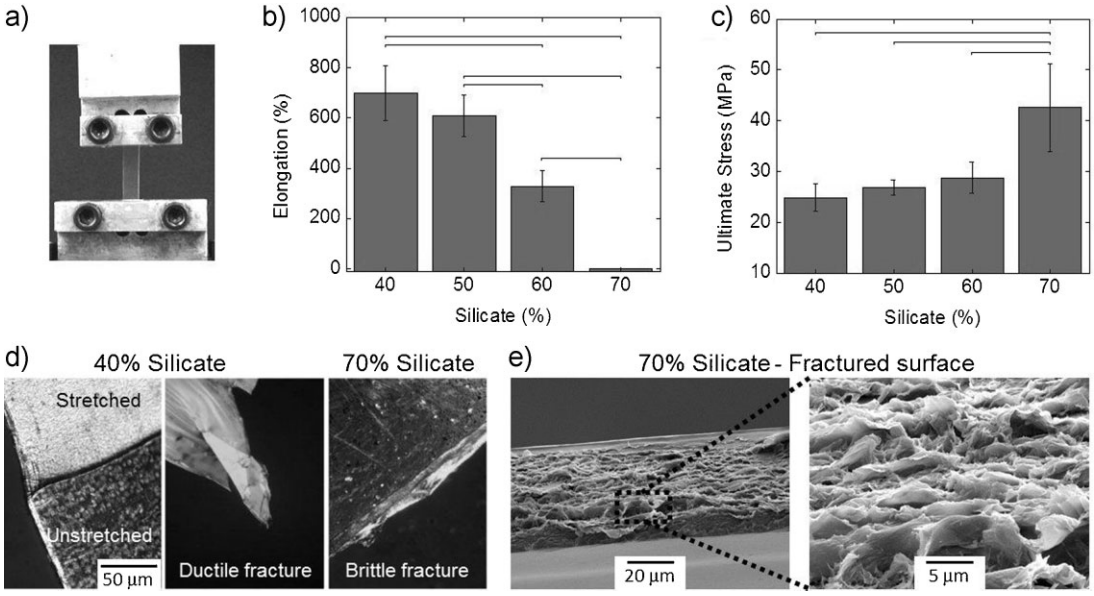

Figure 7. Effect of silicate on mechanical properties of dried nanocomposite films. (a) Dried nanocomposite film used for uniaxial tensile testing. (b), (c) The increase in silicate concentration decreases elongation and increases ultimate stress. Statistical significance ($p < 0.05$) between the groups is indicated by bars. (d) Polarized microscopic images showing fractured regions of the nanocomposite films containing low (40%) and high (70%) silicate concentrations. At low silicate concentrations, nanocomposite films show ductile fracture, whereas at high silicate concentrations brittle fracture was observed. (e) Scanning electron microscopy of the fractured regions of the nanocomposite films containing 70% silicate suggest deformation of layered structures. The ordered structures observed in the films are responsible for high mechanical strength and lower elongation.

nanoparticles, stretch and possibly detach from the silicate crosslinkers, thereby resulting in extensive elongation. As the silicate concentration is increased, the total elongation decreases and tensile stress increases, because a larger proportion of polymer chains directly interacts with the silicate crosslinker.

Similar results were reported by Perotti et al. in bacterial cellulose (BC)/Laponite nanocomposites.[65] They observed that addition of Laponite to BC fibrils significantly enhanced the Young's modulus and tensile strength of the nanocomposite films. The increase in the mechanical strength of the films was attributed to strong hydrogen bonding between inorganic nanoparticles and organic BC fibrils.[65] In another study, Khunawattanakul et al. evaluated chitosan/silicate nanocomposite films to modulate drug release.[66] They observed that addition of silicate nanoparticles retarded film erosion and prolonged drug release. In a similar study, Lee et al. also attributed significant increase in elastic moduli of nanocomposite films to enhanced surface interactions between silicate nanoparticles and polymer (isosorbide polycarbonate).[67]

Our data suggest that at lower silicate concentrations (40, 50, and 60%) nanocomposite films exhibit ductile fracture as evaluated by the polarized microscopy. The birefringence observed in the nanocomposite films can be attributed to the microstructure alignment that results from mechanical deformation. At high silicate concentrations (70%), visible deformation and alignment of the network structure were suggested only near the fractured edge (Figure 7d). As seen by electron microscopy, the fractured edge of the nanocomposite films (70% silicate) consisted of deformed layered structures (Figure 7e). The unique layered structures observed are responsible for high mechanical strength and low elongation in these nancomposite films.

3.8. Silicate Enhances Adhesion and Spreading of hMSCs

A general requirement to develop a material for tissue engineering application is that it should support cell adhesion and spreading. Cell adhesion plays a strong role in cell spreading, migration, proliferation, differentiation, and formation of the extracellular matrix (ECM). hMSCs have shown potential in tissue engineering as they can differentiate into different cell types (osteoblasts, chondrocytes, and adipocytes).[68] In order to evaluate the potential of silicate crosslinked PEO nanocomposite for tissue engineering applications, in vitro cell culture studies were performed to evaluate the adhesion, proliferation, and differentiation of hMSCs on nanocomposites surfaces.

The biological properties of nanocomposite films are strongly influenced by the hydration degree and mechanical properties. Earlier we had shown that dried nanocompsoites films readily hydrate in physiological

conditions and reaches equlibrium within 6 h.[31,60] The equlibrium water content of fully hydrated films are 91 ± 9, 88 ± 8, 83 ± 10, and 67 ± 12% for the nanocomposite films containing 40, 50, 60, and 70% silicate, respectively, in PBS at 37 °C. Similarly, addition of silicate also influences long-term physiological stability of these nanocomposite films. All the nanocomposite compositions show steady weight loss up to 21 d. In vitro degradation/dissolution study indicates weight loss of 47 ± 1.2, 43.5 ± 3.5, 27.5 ± 1.4, and 22.7 ± 7.8% for nanocomposites containing 40, 50, 60, and 70% silicate, respectively. Moreover, we also reported that addition of silicate significantly enhances elastic modulus (G') and loss modulus (G'') of fully hydrated nanocomposite films.[31] This indicates that addition of silicate results in formation of physiologically stable network. It can be expected that cell adhesion, proliferation, and differentiation can also be indirectly influenced by the physical properties of hydrated nanocomposites.

The nanocomposite films with low silicate concentration do not support cell adhesion and spreading. On the other hand, hMSCs readily attach and spread on nanocomposites with high silicate concentration (Figure 8). A strong correlation between silicate concentration and cytoskeleton organization was observed. At low silicate concentration, the hMSCs display round/spherical morphology due to poor cell/matrix interaction. However, at higher silicate concentration, a well organized cytoskeleton with stressed fiber was observed. Together, these results reveal that cell adhesion, spreading, and cytoskeletal organization can be controlled by silicate concentration.

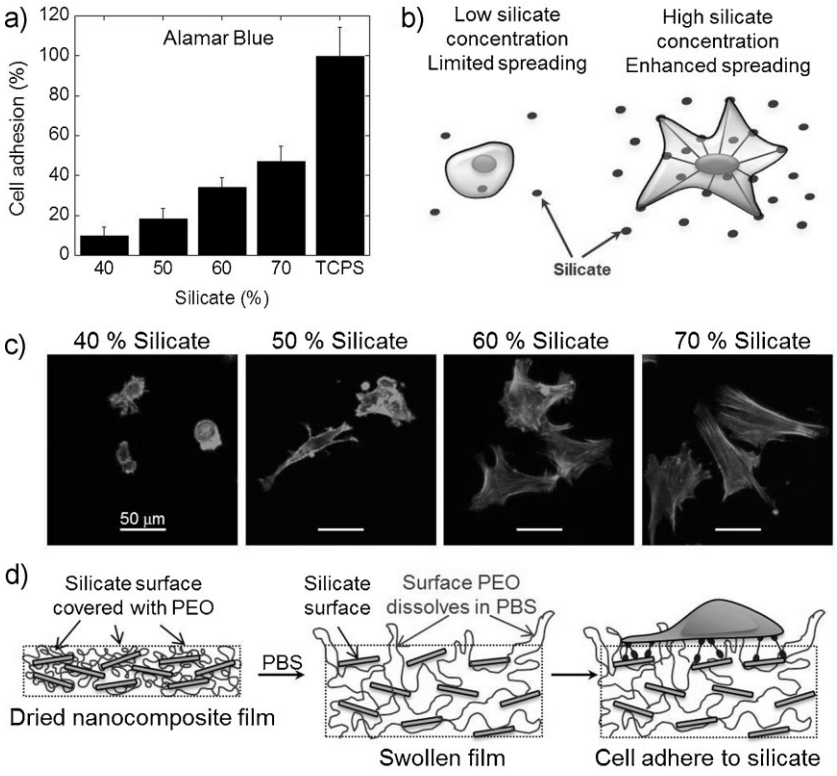

Figure 8. Effect of silicate on adhesion and spreading of hMSCs. (a) Effect of silicate on adhesion on hMSCs is clearly visible. When silicate concentration is increased from 40 to 70% more than fourfold increase in initial cell adhesion was observed. This indicates that silicate may be responsible for initial cell adhesion. (c) Cell spreading was determined after 3 h postseeding. A concentration depend trend was observed, indicating that silicate facilitates cell spreading possibly by providing addition cell adhesion sites. (d) Schematic showing proposed cell adhesion and spreading mechanism. When dried nanocomposite film is exposed to PBS, PEO chains quickly hydrate due to their hydrophilic nature. This results in exposure of silicate surface which act as cell adhesion sites. Cell adhesion is significantly different ($p < 0.05$) on nanocomposites containing 60 and 70% silicate compared to nanocomposites containing 40 and 50% silicate and the positive control (TCPS).

There are two possible mechanisms by which the concentration of silicate may influence the adhesion and spreading of hMSCs. First, silicate allows protein adsorption and cells attach to the proteins. The changes in the topography of the nanocomposite based on the concentration of silicate as evidenced by SEM may affect the adhesion and spreading of hMSCs because many proteins can attach to many silicate nanoparticles. Previous studies have shown that mammalian cells can recognize changes in the nanostructure which in turn may affect cell adhesion, spreading, proliferation, and differentiation.[69,70] It is likely that the layered structure of the nanocomposite due to the presence of with high concentration of silicate better supports the adhesion and spreading of hMSCs. Second, the silicate nanoparticles may act as focal adhesion sites for the cells. Therefore, higher the concentration of silicate, more the number of available attachment sites for the cells to adhere and spread. These attachment sites are initially masked by the PEO chains; however, when the nanocomposite films are hydrated in a physiological environment, the PEO chains undergo adsorption and desorption on the silicate surface due to ionic interaction and hydrogen bonding thereby exposing the silicate surfaces and allowing the cells to interact and attach on the nanoparticles. These results are in agreement with our previous studies which show that the concentration of silicate can be used to control adhesion and spreading of fibroblasts[35,60] and osteoblast cells.[31,61] In a recent study, Chang et al. have also demonstrated that the addition of silicate to covalently crosslinked PEG network enhances hMSCs adhesion.[30]

3.9. hMSCs Readily Proliferate on Nanocomposites

Effect of silicate concentration on proliferation of hMSCs on nanocomposites was evaluated using Alamar Blue assay and the results are shown in Figure 9. Due to low protein adsorption and reduced cell adhesion, PEO by itself does not promote cell growth.[71] In nanocomposites containing low concentration of silicate (40 and 50%), PEO chains dominate and hence very limited cell growth was observed over a period of two weeks. However, at higher silicate concentrations (60 and 70%), enhanced cell proliferation was observed suggesting that silicate not only supports cell adhesion and spreading but also promotes cell proliferation. On days 9 and 12, cell growth reaches a plateau phase on nanocomposites containing 60 and 70% silicate indicating that the cells have grown to confluency.

To visually examine cell morphology by the end of the culture, cell seeded films were fixed and the actin filaments were stained with AlexaFluor Phalloidin (Figure 9a). Confocal images of the stained cells revealed that on nanocomposites with 70% silicate concentration, cells grow into a confluent monolayer by day 12. On the contrary, nanocomposite films containing low amount of silicate were sparsely populated with cells that exhibited spherical or round shape morphology. These results indicate that addition of silicate nanoparticles to PEO significantly enhances the proliferation of hMSCs.

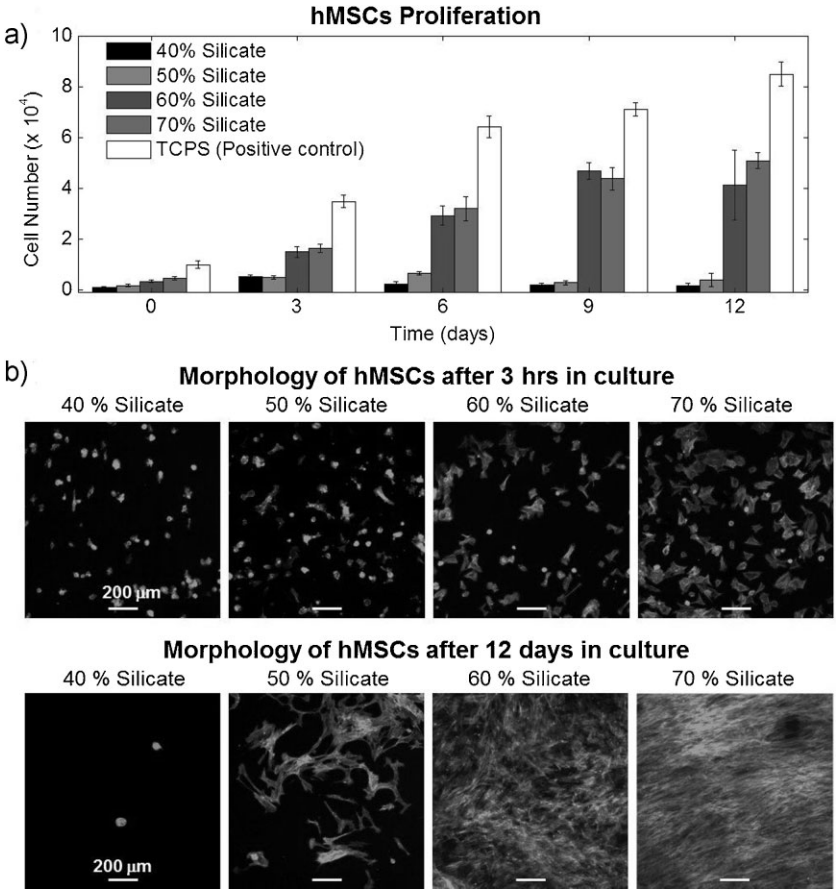

Figure 9. Effect of silicate on hMSCs proliferation. (a) Proliferation of hMSCs was monitored on nanocomposite films containing different amount of silicate for 2 weeks using alamar blue assay. The nanocomposite films containing low amount of silicate show negligible cell growth. At higher silicate concentration (60 and 70%), hMSCs readily grow and proliferate. (b) Visual examination of the morphology of hMSCs on nanocomposite films was done by staining the cytoskeleton of the cells after 3 h and 2 weeks of in vitro culture. hMSCs seeded on nanocomposite containing low silicate concentration show minimum growth due limited cell spreading. The increase in silicate concentration leads to formation of a confluent monolayer of cells. Cell number on nanocomposites containing 60 and 70% silicate are significantly different ($p < 0.05$) than nancomposite containing 40 and 50% silicate and the positive control (TCPS).

The proliferation results correlate well with cell adhesion and spreading findings suggesting that these are interdependent. Both intracellular signaling and phenotypic fate of hMSCs are directly affected by integrin binding and mechanotransduction that control cell shape. It has been previously shown that cell shape regulates cell growth, viability,[72] and differentiation of hMSCs.[73] The flattened and spread out cells promote osteogenesis while unspread and round cells promote the formation of adipocytes.

3.10. Silicate Promotes the Osteogenic Differentiation of hMSCs

Bioactive materials interact with cells by eluting soluble components and influence cellular function. For example, the ionic dissolution products of bioactive glass have been shown to stimulate osteogenesis, angiogenesis, and antimicrobial properties.[22] Xynos et al. showed that media conditioned with bioactive glass containing very high silicon concentration upregulated the expression of 60 genes that are directly related to osteoblast proliferation and differentiation.[74] Silicate nanoparticles have been shown to degrade into non-toxic products [Na^+, $Si(OH)_4$, Mg^{2+}, Li^+] between pH = 7.3 and 8.4.[23] On basis of these studies, it is expected that silicate-based nanocomposites will promote osteogenic differentiation of hMSCs by providing ionic dissolution products.

Runt-related transcription factor-2 (Runx2) and Osteocalcin are key markers for osteogenesis.[75,76] Quantitative

RT-PCR results revealed that while the expression of Runx2 was lower on nanocomposite films at day 7, the expression of osteocalcin was 1.5–2-fold higher on nanocomposite films compared to the TCPS control (Figure 10). At day 10, the expression of both Runx2 and osteocalcin increased on the TCPS surface compared to day 7. The expression of osteocalcin on the nanocomposite films was maintained from day 7 to 10. Runx2, an early marker of osteogenesis, is a key transcription factor that regulates the expression of various genes like osteocalcin and osteopontin that are involved in osteoblast differentiation.[75] Previous studies have shown that after an initial upregulation, the expression of Runx2 decreases progressively with time during osteoblast differentiation.[77,78] The decrease in the expression of Runx2 has been observed to correlate with the upregulation of osteocalcin expression. In the current study, it is likely that the Runx2 expression is on the decline on the nanocomposite films at day 7. Osteocalcin is produced by osteoblasts and is a specific marker for osteoblast differentiation. The early upregulation of osteocalcin (day 7) on nanocomposite films compared to the TCPS control may suggest that the presence of silicate expedites the differentiation of hMSCs toward the osteogenic lineage.

Overall, these preliminary data suggest that silicate crosslinked PEO nanocomposite have the potential to effectively promote the osteogenic differentiation of hMSCs. These results are in agreement with several studies that indicate that the addition of bioactive nanoparticles (silica and hydroxyapatite) to polymeric matrix upregulates the expression of osteogenic differentiation genes. Mieszawska et al. fabricated biodegradable and osteoinductive nano- and micro-composites from silk fibroin and silica particles and reported that the addition of silica nanoparticles upregulates the production of bone sialoprotein (BSP) and type I collagen.[79] In another study, Lee et al. reported that addition of bioactive nanoparticles (hydroxyapatite) to polymeric matrix (PLGA) significantly enhances expression of alkaline phosphatase and osteocalcin in hMSCs.[80] They observed that the addition of hydroxyapatite nanoparticles provide a unique microenvironment to promote osteogenic differentiation and formation of mineralized matrix.

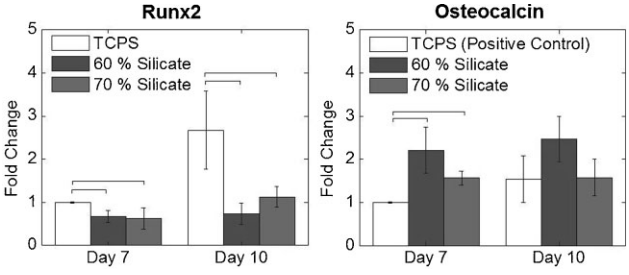

Figure 10. Effect of silicate on osteogenic differentiation of hMSCs. The upregulation of osteocalcin on silicate crosslinked PEO nanocomposites at day 7 indicates that they have the potential to promote osteogenic differentiation of hMSCs. TCPS acts as a positive control. Statistical significance ($p < 0.05$) between the groups is indicated by bars.

One of the potential applications of silicate-based nanocomposites is to engineer orthopedic tissue interfaces. Interfaces such as bone/cartilage (osteochondral), bone/ligament, and bone/tendon are specialized area playing critical role in transferring mechanical load and biochemical signaling. Here, we have shown that cell/matrix interactions and mechanical properties can be simultaneously tuned by controlling PEO/silicate interactions. Thus by fabricating a gradient scaffold we can mimic the zonal structure observed at the tissue interfaces (such as osteochondral). Additionally, silicate-based materials can be fabricated as microfibers for aligned cell growth.[10] These aligned fibrous scaffolds can potentially be used in bone/tendon tissue engineering.

4. Conclusion

We have prepared and characterized a series of physically crosslinked nanocomposite hydrogels containing silicate nanoparticles and PEO. The silicate nanoparticles (Laponite) physically interact with polymer chains which results in the formation of viscoelastic networks. All the hydrogel compositions reported here show shear thinning characteristics indicating their potential use for minimally invasive therapies. As the silicate concentration is increased, the hydrogel networks become stiff and strong. Dense nanocomposite films are obtained after subjecting the hydrogels to solvent evaporation. At low silicate concentrations, highly extensible films are obtained, whereas high silicate concentrations result in mechanically strong films. Hierarchical microstructures are observed at high silicate concentrations, indicating an ordered arrangement of silicate and polymer. A strong correlation between attachment, spreading, and proliferation of hMSCs with silicate concentration was observed. Preliminary data from differentiation experiments indicate that silicate-based nanocomposites promote osteogenic differentiation of stem cells. Overall, it can be concluded that both physical and biological properties of silicate crosslinked PEO nanocomposites can be tuned by modulating the silicate concentration. These nanocomposites have potential to be used for tissue engineering applications that require controlled cell adhesion or proliferation.

Acknowledgements: This research was supported in part by the Purdue Research Foundation and the Weldon School of Biomedical

Engineering. The authors would also like to thank Dr. Shilpa Sant of MIT for technical discussions.

Received: December 10, 2011; Revised: January 30, 2012; Published online: April 19, 2012; DOI: 10.1002/mabi.201100508

Keywords: human mesenchymal stem cells; mechanical properties; nanocomposites; poly(ethylene oxide); silicate nanoparticles

[1] R. Langer, D. A. Tirrell, *Nature* **2004**, *428*, 487.
[2] E. Engel, A. Michiardi, M. Navarro, D. Lacroix, J. A. Planell, *Trends Biotechnol.* **2008**, *26*, 39.
[3] R. A. Hule, D. J. Pochan, *MRS Bull.* **2007**, *32*, 354.
[4] J. I. Dawson, J. M. Kanczler, X. B. Yang, G. S. Attard, R. O. C. Oreffo, *Adv. Mater.* **2011**, *23*, 3304.
[5] H. D. Wagner, *Nat. Nanotechnol.* **2007**, *2*, 742.
[6] N. S. Satarkar, D. Biswal, J. Z. Hilt, *Soft Matter* **2010**, *6*, 2364.
[7] P. Schexnailder, G. Schmidt, *Colloid Polym. Sci.* **2009**, *287*, 1.
[8] P. Fratzl, R. Weinkamer, *Prog. Mater. Sci.* **2007**, *52*, 1263.
[9] S. Mitragotri, J. Lahann, *Nat. Mater.* **2009**, *8*, 15.
[10] A. K. Gaharwar, P. J. Schexnailder, A. Dundigalla, J. D. White, C. R. Matos-Pérez, J. L. Cloud, S. Seifert, J. J. Wilker, G. Schmidt, *Macromol. Rapid Commun.* **2011**, *32*, 50.
[11] L. J. Bonderer, A. R. Studart, L. J. Gauckler, *Science* **2008**, *319*, 1069.
[12] K. Haraguchi, T. Takehisa, *Adv. Mater.* **2002**, *14*, 1120.
[13] P. Podsiadlo, A. K. Kaushik, E. M. Arruda, A. M. Waas, B. S. Shim, J. Xu, H. Nandivada, B. G. Pumplin, J. Lahann, A. Ramamoorthy, N. A. Kotov, *Science* **2007**, *318*, 80.
[14] S. M. Liff, N. Kumar, G. H. McKinley, *Nat. Mater.* **2007**, *6*, 76.
[15] A. K. Gaharwar, S. A. Dammu, J. M. Canter, C.-J. Wu, G. Schmidt, *Biomacromolecules* **2011**, *12*, 1641.
[16] C.-J. Wu, A. K. Gaharwar, P. J. Schexnailder, G. Schmidt, *Materials* **2010**, *3*, 2986.
[17] A. Okada, A. Usuki, *Macromol. Mater. Eng.* **2006**, *291*, 1449.
[18] R. A. Vaia, E. P. Gianellis, *MRS Bull.* **2001**, *62*, 394.
[19] C.-J. Wu, A. K. Gaharwar, B. K. Chan, G. Schmidt, *Macromolecules* **2011**, *44*, 8215.
[20] L. L. Hench, *J. Eur. Ceram. Soc.* **2009**, *29*, 1257.
[21] L. L. Hench, H. A. Paschall, *J. Biomed. Mater. Res.* **1973**, *7*, 25.
[22] A. Hoppe, N. S. Güldal, A. R. Boccaccini, *Biomaterials* **2011**, *32*, 2757.
[23] D. W. Thompson, J. T. Butterworth, *J. Colloid Interface Sci.* **1992**, *151*, 236.
[24] K. R. Martin, *J. Nutr. Health Aging* **2007**, *11*, 94.
[25] E. M. Carlisle, *Science* **1970**, *167*, 279.
[26] D. M. Reffitt, N. Ogston, R. Jugdaohsingh, H. F. J. Cheung, B. A. J. Evans, R. P. H. Thompson, J. J. Powell, G. N. Hampson, *Bone* **2003**, *32*, 127.
[27] Y. Li, D. Maciel, H. Tomas, J. Rodrigues, H. Ma, X. Shi, *Soft Matter* **2011**, *7*, 6231.
[28] V. Tzitzios, G. Basina, A. Bakandritsos, C. G. Hadjipanayis, H. Mao, D. Niarchos, G. C. Hadjipanayis, J. Tucek, R. Zboril, *J. Mater. Chem.* **2010**, *20*, 5418.
[29] Y. S. Pek, M. Kurisawa, S. Gao, J. E. Chung, J. Y. Ying, *Biomaterials* **2009**, *30*, 822.
[30] C.-W. Chang, A. van Spreeuwel, C. Zhang, S. Varghese, *Soft Matter* **2010**, *6*, 5157.
[31] A. K. Gaharwar, P. J. Schexnailder, B. Kline, G. Schmidt, *Acta Biomater.* **2011**, *7*, 568.
[32] A. K. Gaharwar, C. P. Rivera, C.-J. Wu, G. Schmidt, *Acta Biomater.* **2011**, *7*, 4139.
[33] G. Schmidt, A. I. Nakatani, C. C. Han, *Rheol. Acta* **2002**, *41*, 45.
[34] G. Schmidt, A. I. Nakatani, P. D. Butler, C. C. Han, *Macromolecules* **2002**, *35*, 4725.
[35] A. K. Gaharwar, P. Schexnailder, V. Kaul, O. Akkus, D. Zakharov, S. Seifert, G. Schmidt, *Adv. Funct. Mater.* **2010**, *20*, 429.
[36] A. Dundigalla, S. Lin-Gibson, V. Ferreiro, M. M. Malwitz, G. Schmidt, *Macromol. Rapid Commun.* **2005**, *26*, 143.
[37] M. J. Hey, S. M. Ilett, G. Davidson, *J. Chem. Soc., Faraday Trans.* **1995**, *91*, 3897.
[38] J. Maxfield, I. W. Shepherd, *Polymer* **1975**, *16*, 505.
[39] G. Schmidt, A. I. Nakatani, P. D. Butler, A. Karim, C. C. Han, *Macromolecules* **2000**, *33*, 7219.
[40] H. A. Baghdadi, E. C. Jensen, N. Easwar, S. R. Bhatia, *Rheol. Acta* **2008**, *47*, 121.
[41] H. A. Baghdadi, H. Sardinha, S. R. Bhatia, *J. Polym. Sci., Part B: Polym. Phys.* **2005**, *43*, 233.
[42] J. D. Kretlow, L. Klouda, A. G. Mikos, *Adv. Drug Delivery Rev.* **2007**, *59*, 263.
[43] L. S. Nair, C. T. Laurencin, M. Tandon, "*Injectable Hydrogels as Biomaterials*", John Wiley & Sons, Hoboken **2010**, p. 179.
[44] L. Yu, J. Ding, *Chem. Soc. Rev.* **2008**, *37*, 1473.
[45] Q. Jin, P. Schexnailder, A. K. Gaharwar, G. Schmidt, *Macromol. Biosci.* **2009**, *9*, 1028.
[46] E. Loizou, P. Butler, L. Porcar, E. Kesselman, Y. Talmon, A. Dundigalla, G. Schmidt, *Macromolecules* **2005**, *38*, 2047.
[47] E. Loizou, P. D. Butler, L. Porcar, Y. Talmon, E. Kesselman, G. Schmidt, *Macromolecules* **2005**, *38*, 2047.
[48] J. L. Drury, D. J. Mooney, *Biomaterials* **2003**, *24*, 4337.
[49] J. Kopecek, *Biomaterials* **2007**, *28*, 5185.
[50] K. S. Anseth, C. N. Bowman, L. Brannon-Peppas, *Biomaterials* **1996**, *17*, 1647.
[51] Q. Zhang, L. A. Archer, *Langmuir* **2002**, *18*, 10435.
[52] A. Loiseau, J.-F. Tassin, *Macromolecules* **2006**, *39*, 9185.
[53] E. Loizou, P. Butler, L. Porcar, G. Schmidt, *Macromolecules* **2006**, *39*, 1614.
[54] A. Nelson, T. Cosgrove, *Langmuir* **2004**, *20*, 10382.
[55] A. Nelson, T. Cosgrove, *Langmuir* **2004**, *20*, 2298.
[56] J. L. Koenig, A. C. Angood, *J. Polym. Sci., Part B: Polym. Phys.* **1970**, *8*, 1787.
[57] B. Tigges, C. Popescu, O. Weichold, *Soft Matter* **2011**, *7*, 5391.
[58] W.-C. Lin, A. Marcellan, D. Hourdet, C. Creton, *Soft Matter* **2011**, *7*, 6578.
[59] X. Li, S. L. Hsu, *J. Polym. Sci.: Polym. Phys. Ed.* **1984**, *22*, 1331.
[60] P. J. Schexnailder, A. K. Gaharwar, R. L. Bartlett Ii, B. L. Seal, G. Schmidt, *Macromol. Biosci.* **2010**, *10*, 1416.
[61] A. K. Gaharwar, P. J. Schexnailder, Q. Jin, C.-J. Wu, G. Schmidt, *ACS Appl. Mater. Interfaces* **2010**, *2*, 3119.
[62] A. Sellinger, P. M. Weiss, A. Nguyen, Y. Lu, R. A. Assink, W. Gong, C. J. Brinker, *Nature* **1998**, *394*, 256.
[63] Z. Tang, N. A. Kotov, S. Magonov, B. Ozturk, *Nat. Mater.* **2003**, *2*, 413.
[64] R. Wang, H. S. Gupta, *Ann. Rev. Mater. Res.* **2011**, *41*, 41.
[65] G. F. Perotti, H. S. Barud, Y. Messaddeq, S. J. L. Ribeiro, V. R. L. Constantino, *Polymer* **2011**, *52*, 157.
[66] W. Khunawattanakul, S. Puttipipatkhachorn, T. Rades, T. Pongjanyakul, *Int. J. Pharm.* **2011**, *407*, 132.
[67] C.-H. Lee, M. Kato, A. Usuki, *J. Mater. Chem.* **2011**, *21*, 6844.

[68] M. F. Pittenger, A. M. Mackay, S. C. Beck, R. K. Jaiswal, R. Douglas, J. D. Mosca, M. A. Moorman, D. W. Simonetti, S. Craig, D. R. Marshak, *Science* **1999**, *284*, 143.
[69] M. J. Dalby, N. Gadegaard, R. Tare, A. Andar, M. O. Riehle, P. Herzyk, C. D. W. Wilkinson, R. O. C. Oreffo, *Nat. Mater.* **2007**, *6*, 997.
[70] C. J. Bettinger, R. Langer, J. T. Borenstein, *Angew. Chem. Int. Ed.* **2009**, *48*, 5406.
[71] J. M. Harris, "*Poly(ethylene glycol) Chemistry: Biotechnical and Biomedical Applications*", Plenum Press, New York, London **1992**.
[72] C. S. Chen, M. Mrksich, S. Huang, G. M. Whitesides, D. E. Ingber, *Science* **1997**, *276*, 1425.
[73] R. McBeath, D. M. Pirone, C. M. Nelson, K. Bhadriraju, C. S. Chen, *Dev. Cell* **2004**, *6*, 483.
[74] I. D. Xynos, A. J. Edgar, L. D. K. Buttery, L. L. Hench, J. M. Polak, *J. Biomed. Mater. Res.* **2001**, *55*, 151.
[75] B. A. Byers, R. E. Guldberg, A. J. Garcia, *Tissue Eng.* **2004**, *10*, 1757.
[76] A. K. Ekaputra, Y. Zhou, S. M. K. Cool, D. W. Hutmacher, *Tissue Eng. Part A* **2009**, *15*, 3779.
[77] G. Wang, L. Zheng, H. Zhao, J. Miao, C. Sun, N. Ren, J. Wang, H. Liu, X. Tao, *Tissue Eng. Part A.* **2011**, *17*.
[78] S. Pregizer, S. K. Baniwal, X. Yan, Z. Borok, B. Frenkel, *J. Cell. Biochem.* **2008**, *105*, 965.
[79] A. J. Mieszawska, N. Fourligas, I. Georgakoudi, N. M. Ouhib, D. J. Belton, C. C. Perry, D. L. Kaplan, *Biomaterials* **2010**, *31*, 8902.
[80] J. H. Lee, N. G. Rim, H. S. Jung, H. Shin, *Macromol. Biosci.* **2010**, *10*, 173.